The dynamics of liquid drops and their interaction with solids of varying wettabilities

Shikhmurzaev, Yulii; Sprittles, James

J. E. Sprittles and Y. D. Shikhmurzaev

Related Articles

Additional information on Phys. Fluids

The dynamics of liquid drops and their interaction with solids of varying wettabilities

J. E. Sprittles[1,a)] and Y. D. Shikhmurzaev[2,b)]
[1]*Mathematical Institute, University of Oxford, Oxford OX1 3LB, United Kingdom*
[2]*School of Mathematics, University of Birmingham, Birmingham B15 2TT, United Kingdom*

Microdrop impact and spreading phenomena are explored as an interface formation process using a recently developed computational framework. The accuracy of the results obtained from this framework for the simulation of high deformation free-surface flows is confirmed by a comparison with previous numerical studies for the large amplitude oscillations of free liquid drops. Our code's ability to produce high resolution benchmark calculations for dynamic wetting flows is then demonstrated by simulating microdrop impact and spreading on surfaces of greatly differing wettability. The simulations allow one to see features of the process which go beyond the resolution available to experimental analysis. Strong interfacial effects which are observed at the microfluidic scale are then harnessed by designing surfaces of varying wettability that allow new methods of flow control to be developed. © *2012 American Institute of Physics*. [http://dx.doi.org/10.1063/1.4739933]

I. INTRODUCTION

The impact and spreading of liquid drops on solid substrates is the key element of a range of technological processes. Examples include spray cooling of surfaces, crop spraying, spray coating, and solder jetting.[1–3] Thus far, research activity has been overwhelmingly devoted to the behaviour of millimetre-sized drops[4–6] where the spatio-temporal scales of interest allow experiments to be performed routinely.[7] However, increasingly, there is an interest in the dynamics of microdrops, whose behaviour is critical to the functioning of a number of microfluidic devices.[8] The ink-jet printer is one such device which, as well as being utilized in the graphic arts, is beginning to become a viable alternative to traditional fabrication methods,[9–12] such as in the cost effective printing of P-OLED displays[13] or the building of complex 3D structures through additive manufacturing.[14] In such processes, the interaction of the microdrops with the solid substrate on which it impacts is directly related to the quality of the product, so that it is important to be able to predict and understand the behaviour of microdrops in such situations.

Much research, currently confined to the millimetre scale, has focused on how the wettability of a solid can dramatically influence a drop's dynamics[15] and how surfaces can be designed with areas of high and low wettability in order to control the spreading of drops on them and enhance the precision of the process to correct for inherent inaccuracies in droplet deposition.[16] Given the even larger surface-to-volume ratio of microdrops, so that surface effects become more dominant, the possibilities for flow control using a pre-patterned solid substrate are significant; however, thus far very few experimental or theoretical papers have addressed this promising new area.

The dynamics of microdrops as they impact on the solid substrate is difficult to observe experimentally,[17,18] especially with a sufficiently high temporal resolution, and characteristics such as the flow field inside the drop or stress acting on the substrate are almost impossible to measure.

---

a)Electronic mail: sprittles@maths.ox.ac.uk.
b)Electronic mail: yulii@for.mat.bham.ac.uk.

24, 082001-1

Therefore, it becomes necessary to rely on a theory which, once validated against the data from experiments on millimetre-sized drops and other relevant free-surface flows, would allow one to obtain reliable information about this process.

So far, the main emphasis in research on microdrop spreading has been on the influence of additional physical effects on the drop's dynamics such as heat and mass transfer;[19] polymeric properties of the liquid;[20] entrapment of bubbles under the drop;[18] spreading on, and imbibition into, porous media;[21,22] evaporation;[23] and solidification.[3] The focus of our research programme is to begin by accurately capturing the process of dynamic wetting, which is the key physical effect in the drop impact phenomenon, and develop a benchmark numerical platform capable of incorporating complex mathematical models that describe the essential features of this process. Once this aspect is resolved, additional physical factors such as heat transfer, interaction with external fields, etc., can be built into the framework as required. An example of one such additional physical effect was given in Refs. 24 and 25, where the model was extended to account for surfaces of inhomogeneous wettability.

The issues surrounding the modelling of dynamic wetting flows are well known and have been the subject of several reviews[26,27] and monographs,[28,29] with a general discussion of the merits and drawbacks of microscopic, mesoscopic, and macroscopic modelling approaches given in Ref. 30 and the discussion notes that followed. A comparison between the different approaches, for example between molecular dynamics simulations, lattice-Boltzmann predictions, and continuum mechanical theories is of significant interest, but is beyond the scope of this paper and would be better conducted on a simpler flow geometry than microdrop impact and spreading, such as, for example, capillary rise in a cylindrical tube. Here, we focus on the self-consistent framework of continuum mechanics where, in particular, it has been established that the classical model of fluid mechanics must be modified to allow for a solution to exist.[26,31,32] A conventional way to achieve this is to use a "slip model" where the no-slip condition is modified to allow for slip between the liquid and the solid near the moving contact line, e.g., using the Navier condition,[33] while the contact angle is prescribed as a function of the contact-line speed and material constants.[34] When incorporated into numerical software, such models have been shown to produce adequate results for the spreading of millimetre-sized drops at relatively low impact speeds, where experiments can be easily analyzed to allow for the development of a semi-empirical analysis of the phenomenon.[35,36]

An open question is whether the models that have been specifically developed for millimetre-sized drop dynamics can predict the behaviour of drops across a range of scales, i.e., towards micro/nanodrops, at a range of impact speeds.

A step in the direction of answering this question was taken in the studies of Refs. 37 and 38. Their results show that, even with millimetre-sized drops, the contact angle is not simply a function of the contact-line speed, but is actually determined by the entire flow field. In other words, the dependence of the contact angle on the contact-line speed for given materials of the system is non-unique; it varies with the speed of impact, i.e., it depends on the particular flow. For an illustration of this effect we refer the reader to Figure 14 in Ref. 37 and Figure 9 in Ref. 38. This effect of the flow field on the contact angle is well known in the process of curtain coating where it has been termed the "hydrodynamic assist of dynamic wetting."[39–41] Similar dependencies of the dynamic contact angle on the flow field have been noted in the spreading of a liquid between parallel plates,[42] the imbibition of liquid into capillaries[43,44] and in the coating of fibres;[45] but these flows are yet to undergo the level of scrutiny that the curtain coating process has where it has been shown, using careful finite element simulations, that the effect cannot be described using any interpretation of the conventional "slip" models.[46] Put simply, all currently available computational software, which implement the "conventional" (i.e., slip) models, are unable to describe this key physical effect which has already been shown to be critical for the optimization of one industrial process and, as experiments suggest, is central to the understanding of microdrop impact and spreading phenomena.

Currently, the only model able to predict the influence of the flow field on the contact angle is the interface formation model. This model is based on the simple physical idea that dynamic wetting, as the very name suggests, is the process in which a fresh liquid–solid interface (a newly "wetted" solid surface) is formed. The model is described in detail in Ref. 29 and has already been shown to be

in agreement with experimental data in a range of different physical phenomena.[24,25,47–52] Notably, recent benchmark simulations for the technologically relevant phenomenon of a liquid-gas meniscus propagating through a cylindrical capillary tube[53] confirm that by modelling dynamic wetting as an interface formation process, we are able to demonstrate the effect of the flow field on the contact angle so that the aforementioned flows exhibiting assist-like behaviour can now be studied using our computational tool.

A further advantage of the interface formation model over conventional approaches is that it is able to naturally account for the influence of variations in the wettability of the solid surface on the bulk flow. Specifically, even when there is no free surface present, the interface formation model predicts that a single[24] or multiple[25] changes in the wettability of the solid substrate can disrupt a shear flow parallel to that solid. The obtained results are in qualitative agreement with the predictions of molecular dynamics simulations[54,55] and will become more important as the scale of the flow is reduced, i.e., as we consider micro and nanofluidic flows.

Computation of dynamic wetting flows is complex: besides the effects of capillarity, viscosity, and inertia, one must also capture the physics of wetting which typically occurs on a length scale much smaller than that of the bulk flow. As explained in detail in Ref. 56, the majority of publications in the field fail to accurately account for the wetting dynamics on the smaller length scale and, consequently, make it impossible to distinguish physical effects from numerical errors in their results. Such codes may provide realistically looking results for millimetre-sized drops, where the accurate computation of the bulk dynamics may be sufficient, but on the micro/nano scale, where an increasing surface-to-volume ratio means that surface effects become more important, such codes are unreliable as the free surface shape near the contact line, specified by the contact angle, is not accurately determined.

The first steps in the development of a benchmark code for such flows was described in great detail in Ref. 56, where a user-friendly step-by-step guide is provided to allow the reader to reproduce all results. This framework was extended in Ref. 53 to allow for the simulation of dynamic wetting as an interface formation process, with the approach robustly tested by checking its convergence both under mesh refinement, allowing practical recommendations on mesh design to be made, and, in limiting cases, to analytic asymptotic results. Furthermore, the developed computational tool was used to predict new physical effects, such as a new type of dependence of the dynamic contact angle on the flow geometry, and was seen to describe experimental data for the imbibition of a liquid into a capillary tube exceptionally well and significantly better than the Lucas-Washburn approach.[57] This situation is in complete contrast to commercial software which have not been validated as thoroughly for this class of flows and have been shown to converge to the wrong solution for similar flows.[58]

In contrast to the flows considered in Refs. 53 and 56, impacting microdrops undergo extreme changes in shape. Therefore, having outlined the model in Sec. II and the numerical approach in Sec. III, in Sec. IV to verify the code's accuracy for large changes in free surface shape we compare our calculations to a known test-case from the literature of oscillating liquid drops, where reliable results exist for an unsteady problem in which inertia, capillarity, and viscosity are all prominent; it is also a problem of significant interest in its own right.

Having verified the code's ability to accurately simulate the dynamics of liquid drops, in Sec. V we demonstrate its capabilities for drop impact and spreading phenomena. Here, we focus on the main physical effects and, in particular, the influence of a substrate's wettability on an impacting drop's behaviour as well as the ability of our computational tool to extract information that is hidden to experimental analysis and which allows new paths of enquiry to be proposed. Most promisingly, in Sec. VI a novel mechanism of flow control is developed, based on pre-patterning a substrate with regions of high and low wettability, that allows the final shape of the drop to be controlled using only slight alterations in the impact speed.

II. MODELLING OF DYNAMIC WETTING PHENOMENA

Consider the flow of an incompressible Newtonian liquid, of constant density ρ and viscosity μ, surrounded by a dynamically passive gas of a constant pressure p_g, so that the continuity and

momentum balance equations are given by

$$\nabla \cdot \mathbf{u} = 0, \qquad \rho \left[\frac{\partial \mathbf{u}}{\partial t} + \mathbf{u} \cdot \nabla \mathbf{u} \right] = -\nabla p + \mu \nabla^2 \mathbf{u} + \rho \mathbf{g}, \tag{1}$$

where t is time, $\mathbf{u}$ and p are the liquid's velocity and pressure, and $\mathbf{g}$ is the gravitational force density.

The interface formation equations, which act as boundary conditions for the bulk equations (1), and have been described in great detail in Ref. 29, are here simply listed with a very brief description given below. These equations consider interfaces as "surface phases" characterized by the surface density ρ^s, surface velocity $\mathbf{v}^s$ with which the density is transported and the surface tension σ which can be viewed as a "two-dimensional pressure" taken with the opposite sign. On a liquid-gas free surface, we have

$$\frac{\partial f}{\partial t} + \mathbf{v}_1^s \cdot \nabla f = 0, \tag{2}$$

$$\mu \mathbf{n} \cdot \left[\nabla \mathbf{u} + (\nabla \mathbf{u})^T \right] \cdot (\mathbf{I} - \mathbf{nn}) + \nabla \sigma_1 = \mathbf{0}, \qquad p_g - p + \mu \mathbf{n} \cdot \left[\nabla \mathbf{u} + (\nabla \mathbf{u})^T \right] \cdot \mathbf{n} = \sigma_1 \nabla \cdot \mathbf{n}, \tag{3}$$

$$\rho \left(\mathbf{u} - \mathbf{v}_1^s \right) \cdot \mathbf{n} = \left(\rho_1^s - \rho_{1e}^s \right) \tau^{-1}, \qquad \frac{\partial \rho_1^s}{\partial t} + \nabla \cdot \left(\rho_1^s \mathbf{v}_1^s \right) = -\left(\rho_1^s - \rho_{1e}^s \right) \tau^{-1}, \tag{4}$$

$$4\beta \left(\mathbf{v}_{1||}^s - \mathbf{u}_{||} \right) = (1 + 4\alpha\beta) \nabla \sigma_1, \qquad \sigma_1 = \gamma(\rho_{(0)}^s - \rho_1^s), \tag{5}$$

where the *a priori* unknown free surface is $f(\mathbf{r}, t) = 0$, with the inward normal $\mathbf{n} = \frac{\nabla f}{|\nabla f|}$, the metric tensor of the coordinate system is $\mathbf{I}$ and the subscript $||$ denotes components parallel to the surface, which are obtained by convolution with the tensor $(\mathbf{I} - \mathbf{nn})$. Subscripts 1 and 2 refer to variables on the free surface and liquid-solid interface, respectively. At a stationary liquid–solid interface, the equations of interface formation have the form

$$\mathbf{v}_2^s \cdot \mathbf{n} = 0, \qquad \mu \mathbf{n} \cdot \left[\nabla \mathbf{u} + (\nabla \mathbf{u})^T \right] \cdot (\mathbf{I} - \mathbf{nn}) + \tfrac{1}{2} \nabla \sigma_2^s = \beta \mathbf{u}_{||}, \tag{6}$$

$$\rho \left(\mathbf{u} - \mathbf{v}_2^s \right) \cdot \mathbf{n} = \left(\rho_2^s - \rho_{2e}^s \right) \tau^{-1}, \qquad \frac{\partial \rho_2^s}{\partial t} + \nabla \cdot \left(\rho_2^s \mathbf{v}_2^s \right) = -\left(\rho_2^s - \rho_{2e}^s \right) \tau^{-1}, \tag{7}$$

$$\mathbf{v}_{2||}^s - \tfrac{1}{2} \mathbf{u}_{||} = \alpha \nabla \sigma_2, \qquad \sigma_2 = \gamma(\rho_{(0)}^s - \rho_2^s). \tag{8}$$

Boundary conditions (2)–(8) are themselves differential equations along the interfaces and are in need of boundary conditions at the contact line. At a contact line where a free surface meets a solid, we have continuity of surface mass flux and the Young equation,[59] which balances the tangential components of the forces due to surface tensions acting on the contact line and hence determines the dynamic contact angle θ_d:

$$\rho_1^s \left(\mathbf{v}_{1||}^s - \mathbf{U}_c \right) \cdot \mathbf{m}_1 + \rho_2^s \left(\mathbf{v}_{2||}^s - \mathbf{U}_c \right) \cdot \mathbf{m}_2 = 0, \qquad \sigma_2 + \sigma_1 \cos \theta_d = 0. \tag{9}$$

Here $\mathbf{m}_i$ are the unit vectors normal to the contact line and inwardly tangential to surface $i = 1, 2$ and the velocity of the contact line is $\mathbf{U}_c$. The surface tension of the solid-gas interface can easily be incorporated into the model at no additional cost, but is here assumed to be negligible and, even for relatively large estimates of its value, tests show its influence on the drop's dynamics is unimportant in the parameter range considered.

On an axis of symmetry, with normal vector $\mathbf{n}_a$, the usual conditions of impermeability and zero tangential stress are applied,

$$\mathbf{u} \cdot \mathbf{n}_a = 0, \qquad \mathbf{n}_a \cdot \left[\nabla \mathbf{u} + (\nabla \mathbf{u})^T \right] \cdot (\mathbf{I} - \mathbf{n}_a \mathbf{n}_a) = \mathbf{0}, \tag{10}$$

together with conditions on the smoothness of the free surface where it meets such an axis $\mathbf{n} \cdot \mathbf{n}_a = 0$ and the absence of a surface mass source/sink for the interface formation equations $\mathbf{v}_{||}^s \cdot \mathbf{n}_a = 0$.

On the free surface, Eq. (2) is the standard kinematic boundary condition, and the Eqs. (3) express the balances of the tangential and normal stress acting on the interface. On the liquid–solid interface, Eqs. (6) state that the solid is impermeable and that the tangential component of the bulk velocity satisfies a generalized Navier condition which shows that slip on the liquid-facing side of the liquid–solid interface can be generated by both tangential stress *on* the interface, with a coefficient of proportionality β, and variations of surface tension *in* the interface. The model takes into account the mass exchange between the bulk and surface phases, in (4) and (7), that are associated with the relaxation of an interface with surface density ρ^s toward its equilibrium state, for which $\rho^s = \rho_e^s$, on characteristic relaxation time τ. The first equation in (5) and (8) shows that the tangential components $\mathbf{v}_{||}^s$ of the surface velocity $\mathbf{v}^s$ are driven both by the bulk motion of the fluid and by gradients in surface tension along the interface, with the response of the interface to the latter effect characterized by the constant α. The second equation in (5) and (8) is the surface equation of state, which here is taken in its simplest linear form, that determines the dependence of the surface tension along the interface on the surface density, with the constant γ associated with the inverse compressibility of the fluid and $\rho_{(0)}^s$ being the surface density corresponding to zero surface tension, and hence allows one to find the contact angle from the Young equation in (9). Therefore, the mechanism by which assist occurs becomes qualitatively clear: the flow is able to influence the distribution of the surface density along the interfaces and hence the values of the surface tensions at the contact line which determine the contact angle. Estimates for the phenomenological material constants α, β, γ, τ, and $\rho_{(0)}^s$ have been obtained by comparing the theory to experiments in dynamic wetting, e.g., in Ref. 60, and small changes in their values will not change the key physical effects identified for microdrop impact and spreading.

Notably, the wettability of the solid substrate is controlled by the equilibrium surface density on it, i.e., ρ_{2e}^s, which is directly related to the surface tension of the liquid–solid interface via the equation of state (8) and hence to the equilibrium contact angle θ_e via the Young equation (9). Therefore, for a solid of homogeneous wettability, the equilibrium surface density along the liquid–solid interface is given in terms of known constants and the measured equilibrium contact angle as

$$\rho_{2e}^s = \rho_{(0)}^s + (\rho_{(0)}^s - \rho_{1e}^s)\cos\theta_e. \tag{11}$$

Then, as shown in Ref. 24, variations in the wettability of the substrate, leading to $\theta_e = \theta_e(\mathbf{x})$, considered in Sec. VI, can easily be built into the model by prescribing a spatial dependence for ρ_{2e}^s using (11).

III. A COMPUTATIONAL FRAMEWORK FOR DYNAMIC WETTING PHENOMENA

A framework for the simulation of dynamic wetting flows as an interface formation process has been developed in Ref. 53, which builds upon previous work[56] where the approach was formulated for the mathematically less complex conventional models. These papers provide a step-by-step guide to the development of the code, curves for benchmark calculations, and a demonstration of our platform's capabilities, by showing excellent agreement with experiments on capillary rise, so that, here, we shall just recapitulate the main details.

The CFD code is based on the finite element method and uses an arbitrary Lagrangian-Eulerian mesh design[46,61,62] to allow the free surface to be accurately represented while bulk nodes remain free to move (snapshots of the mesh can be seen below in Figure 6). This mesh is based on the bipolar coordinate system and is graded so that exceptionally small elements are used near the contact line to accurately capture the physics of interface formation there (see Ref. 53 for estimates on the smallest element size required for given parameters), while in the bulk of the liquid larger elements are adequate and ensure the resulting problem is computationally tractable. For the problems considered, structured meshing has worked perfectly well, although one can easily envisage flows in which the topology of the domain makes adaptive meshing more appealing. The model is equally valid for three-dimensional phenomena, such as those where contact-line instabilities can trigger fingering and splashing, or oblique impacts, but the computational implementation of the model considered here is restricted to unsteady is two-dimensional flows and thus confines us to considering axisymmetric impacts. The extensions required for the accurate computation of three-dimensional

dynamic wetting phenomena remains a huge computational challenge, as the spatial and temporal scales that must be captured by a numerical scheme (see below) can be exceedingly restrictive. However, as experiments for microdrops show, impacts normal to a solid are axisymmetric so that our current computational code will allow us to identify the key physical effects involved in this process.

The result of our spatial discretization is a system of nonlinear differential algebraic equations of index 2 (Ref. 63) which are solved using the second-order backward differentiation formula, whose application to the Navier-Stokes equations is described in detail in Ref. 64, using a time step which automatically adapts during a simulation to capture the appropriate temporal scale at that instant. For example, the time steps required in the initial stages after impact of the drop are small compared to those used in the later stages where the drop often gently oscillates around its equilibrium position on a much longer characteristic time scale.

The described CFD code has been thoroughly validated for dynamic wetting phenomena, using both conventional models[56] and the interface formation model,[53] in both steady and unsteady regimes, for example for the benchmark test case of the propagation of a meniscus into a capillary where the contact line undergoes a short period of acceleration followed by a long time scale deceleration as the meniscus evolves toward an equilibrium position. In these relatively simple geometries, we have been able to fully validate the dynamic wetting model for all realistic parameters including high capillary number flows, in which the curvature near the contact line is significant. These tests allowed is to identify the mesh resolution required to obtain an accurate solution.

When compared to our previous works, the main difference with microdrop impact and spreading is that very large changes in the entire free surface shape are observed, i.e., the bulk of the drop experiences significant deformation. Therefore, continuing in the spirit of our previous publications, which have already validated the dynamic wetting model for all realistic parameter values, the code is first validated for this class of flows where the bulk undergoes large changes in shape. This, additionally, allows us to demonstrate how easily the framework can be adapted to handle a variety of free surface flows.

IV. OSCILLATING DROPS: VALIDATION OF THE UNSTEADY CODE FOR LARGE FREE-SURFACE DEFORMATION

Consider the free oscillation of liquid drops in a parameter regime that will allow us to test our results against known numerical solutions for a high deformation unsteady flow which exhibits the competing forces of capillarity, inertia, and viscosity. For small oscillations analytic results exist,[65] but for arbitrary viscosity and deformation numerical methods are required. The test case considered is for the standard model, which can be easily obtained from the interface formation model's equations for the free surface (2)–(5) by setting the ratio τ/T of interfacial relaxation time τ to bulk time scale T to zero (see Ref. 53 for details), so that the same code can be used. In this case, the flow is fully characterized by the Reynolds, Stokes, and capillary numbers, which are, respectively,

$$Re = \frac{\rho U L}{\mu}, \qquad St = \frac{\rho g L^2}{\mu U}, \qquad \text{and } Ca = \frac{\mu U}{\sigma_{1e}}, \tag{12}$$

where L and U are the scales for length and velocity, and σ_{1e} is the equilibrium surface tension on the free surface. Here, we consider oscillation in zero-gravity so that $St = 0$.

Parameters are chosen to allow a comparison of our results with the numerical studies reported by other groups in Refs. 66 and 67. To do so, we run two simulations of the axisymmetric oscillation of a drop with $Re = 10, 100$ and $Ca = 0.1, 0.01$ (so that $We = Re\, Ca = 1$ for both simulations), respectively. We consider the oscillation of a viscous liquid droplet whose initial shape is most
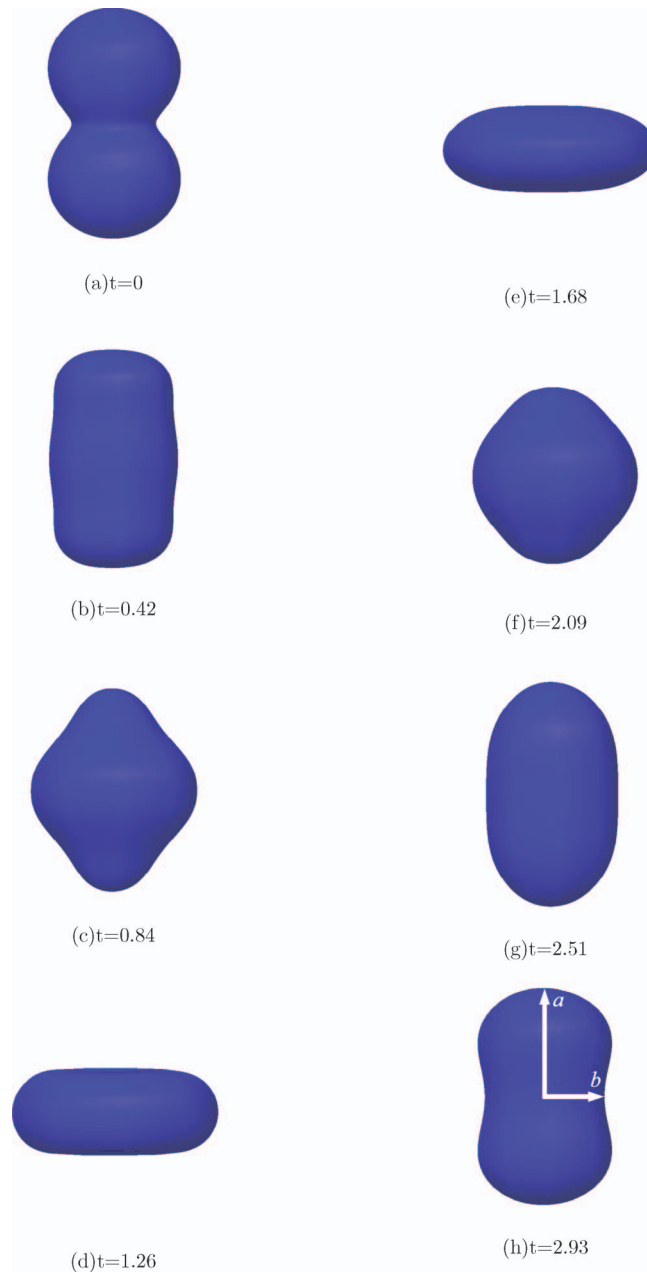
FIG. 1. Evolution of a liquid drop with Re=100 and We=1 over one period ($T = 2.93$).

naturally represented in spherical polar coordinates (R, α, φ), with the origin located at the centre of the drop so that the drop surface $\mathbf{x}_G$ is given by

$$\mathbf{x}_G = f(\alpha, t)\mathbf{e}_R, \tag{13}$$

where $\mathbf{e}_R$ is a unit vector in the radial direction. Then, as shown in Figure 1(h), $a = f(0, t)$ is the length of the semi-major axis and $b = f(\pi/2, t)$ is the length of the semi-minor axis.

In the benchmark test case, the drop is released from a shape whose deviation from a sphere is proportional to the 2nd spherical harmonic $P_2(\cos \alpha) = \frac{1}{2}(3 \cos^2 \alpha - 1)$, with coefficient of proportionality chosen to be 0.9, so that
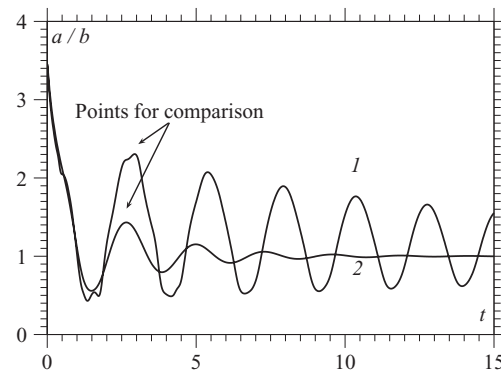
$$f(\alpha, 0) = \gamma[1 + 0.9 P_2(\cos \alpha)], \tag{14}$$

FIG. 2. Aspect ratio a/b of two drops over a number of periods with curve 1 obtained using Re=100, We=1 while curve 2 is for Re=10, We=1.

where γ is a normalizing factor which ensures that the droplet has the correct non-dimensional volume, in our case $\gamma = 4\pi/3$.

We record the time T_1, and aspect ratio of the drop after one period $(a/b)_{T_1}$, for Re = 10, 100 and $We = 1$ in order to validate our code against the previous studies. For the results which are presented, a relatively crude mesh of 630 elements was used with a fixed time step of $\delta t = 0.001$. Doubling the number of elements or reducing the time step by a factor of ten resulted in a change of less than 0.1% in both the time and amplitude recorded after one period. Significantly, the results in Ref. 66 were for 128 elements while Ref. 67 use an order of magnitude more elements.

Figure 1 shows the evolution of the drop over one period for the $Re = 100$ case. The high deformation of the free surface is clear and one can observe that at the end of the first period the drop, whose equilibrium shape is a sphere, has its amplitude of oscillation damped by viscosity. Figure 2 shows the time-dependence of the aspect ratio a/b, which is recorded after one period $t = T$. It should be pointed out that the kinks in curve 1 of Figure 2 are not numerical artifacts; they are associated with the high deformation regime and can be seen in the previous studies.

Our results in Table I are seen to be in good agreement with both studies. The values align most closely with those of Ref. 67, which is reassuring given the greater mesh resolution associated with this study.

Thus, it has been demonstrated that our numerical framework is able to provide accurate results for complex unsteady free-surface flows. The oscillation of liquid drops is a problem of interest in its own right, and at this point we could look at comparing our results to experiments in the literature,[68] to probe newly proposed analytic models for decay rates[69] or to consider the influence that including interface formation physics may have when oscillations are of high frequency and the interface is forming and disappearing at a significant rate. All of these avenues of investigation are being pursued but lie beyond the scope of the present paper, and we now turn our attention to the code's capabilities at describing drop impact and spreading phenomena.

TABLE I. Comparison of current results with previous studies.

Re=10	Ref. 66	Ref. 67	Present work
T_1	2.660	2.640	2.656
$(a/b)_{T_1}$	1.434	1.432	1.432
Re=100			
T_1	2.905	2.930	2.936
$(a/b)_{T_1}$	2.331	2.304	2.305

V. MICRODROP IMPACT AND SPREADING

To study the key physical effects in microdrop impact and spreading phenomena in a range applicable to inkjet printing technologies, we consider simulations of impact on hydrophilic, hydrophobic, and patterned substrates. In particular, we see that our code is able to account for the two extreme outcomes of the drop impact and spreading process, i.e., deposition and rebound; to recover information about the drop's dynamics which is currently unobtainable from purely experimental analysis; and to predict new methods for flow control on chemically patterned surfaces.

Consider a microdrop of water of radius $L = 25$ μm which impacts a solid substrate at $U = 5$ m s^{-1}, with the subsequent motion considered axisymmetric. Then, the non-dimensional parameters are $Re = 130$, $Ca = 0.07$, and $St = 0.001$ and estimates for the interface formation model's parameters are taken from Ref. 60. All that remains to be specified is the wettability of the solid substrate, which is characterized by the equilibrium contact angle θ_e that a free surface forms with the solid.

Two simulations are shown in Figure 3 for the impact of a drop on substrates of different wettabilities, $\theta_e = 60°$ and $\theta_e = 130°$, respectively, with an associated movie in Video 1. The evolutions of the contact line radius r_c and and apex height z_a are given in Figure 4. Hereafter, for brevity we use the term "apex" for the point located at the intersection of the axis of symmetry and the free surface; as Figure 7 shows, it is not necessarily the highest point of the free surface.

In Figure 3, it can be seen that in the early stages of spreading when inertia is dominant, roughly until $t = 1$ (with one dimensionless unit corresponding to 5 μs for the drop on which our non-dimensional parameters were based), the shapes of the two drops are indistinguishable. As can be seen in Figure 5, the contact line is forced outwards as fluid is pushed out radially from the centre of the drop which is being driven vertically into the substrate by inertial forces. This causes a toroidal rim of fluid to form near the contact line, with the pressure plot in Figure 5 clearly showing the formation of a disturbance, travelling from the contact line toward the apex, which separates the growing rim of fluid from the bulk of the drop. Eventually, the drop starts to feel the wettability of the solid on which it is spreading and, since in both cases inertia has carried the drop past its equilibrium position, the contact line starts to recede which, as shown in Figure 4, occurs when the dynamic contact angle drops below its equilibrium value (dashed lines). As expected, when the drop's angle is furthest from equilibrium, the speed of the contact line is fastest. Noticeably, as can be seen in both Figures 3 and 4, although the wettability of the substrate eventually begins to alter the position of the contact line; this is not felt by the apex until a much later time. In fact, the initial fall of the apexes are very similar, and it is only upon their recoil, around $t = 4$, that their paths begins to differ. When the drops begin to recoil, their motions differ quite significantly; notably, for the drop on the hydrophobic substrate, where the dewetting of the substrate occurs so quickly that the drop rebounds back off the substrate. By comparing the images at $t = 3$ and $t = 4$ in Figure 3, one can see that the rebound is preceded by a jet emanating from the apex region which pulls fluid radially inwards toward the axis of symmetry. This second stage of spreading is seen to be on a much longer time scale than the initial stages after impact. The simulation has to be terminated as the drop is about to leave the substrate; extending the numerical platform to account for such behaviour is certainly viable. It is of interest to see that the drop's final shape is pear shaped and, indeed, this shape has been observed experimentally.[70]

Snapshots of the mesh used during the computation of the obtained results are given in Figure 6, where a relatively crude mesh is shown, allowing the elements to be easily identified. One can see that the mesh remains regular throughout extreme changes in free surface shape, like at $t = 3$, when the apex is very close to touching the substrate, and at $t = 10.5$, when the drop is close to leaving the substrate.

Some of our computational framework's advantages over a purely experimental analysis of the phenomenon are as follows. First, it can recover information which is inaccessible to experiments; second, one can efficiently map the influence of the system's parameters on the drop's dynamics, and, third, it is easy to attempt new things without the cost of full scale laboratory experiments.
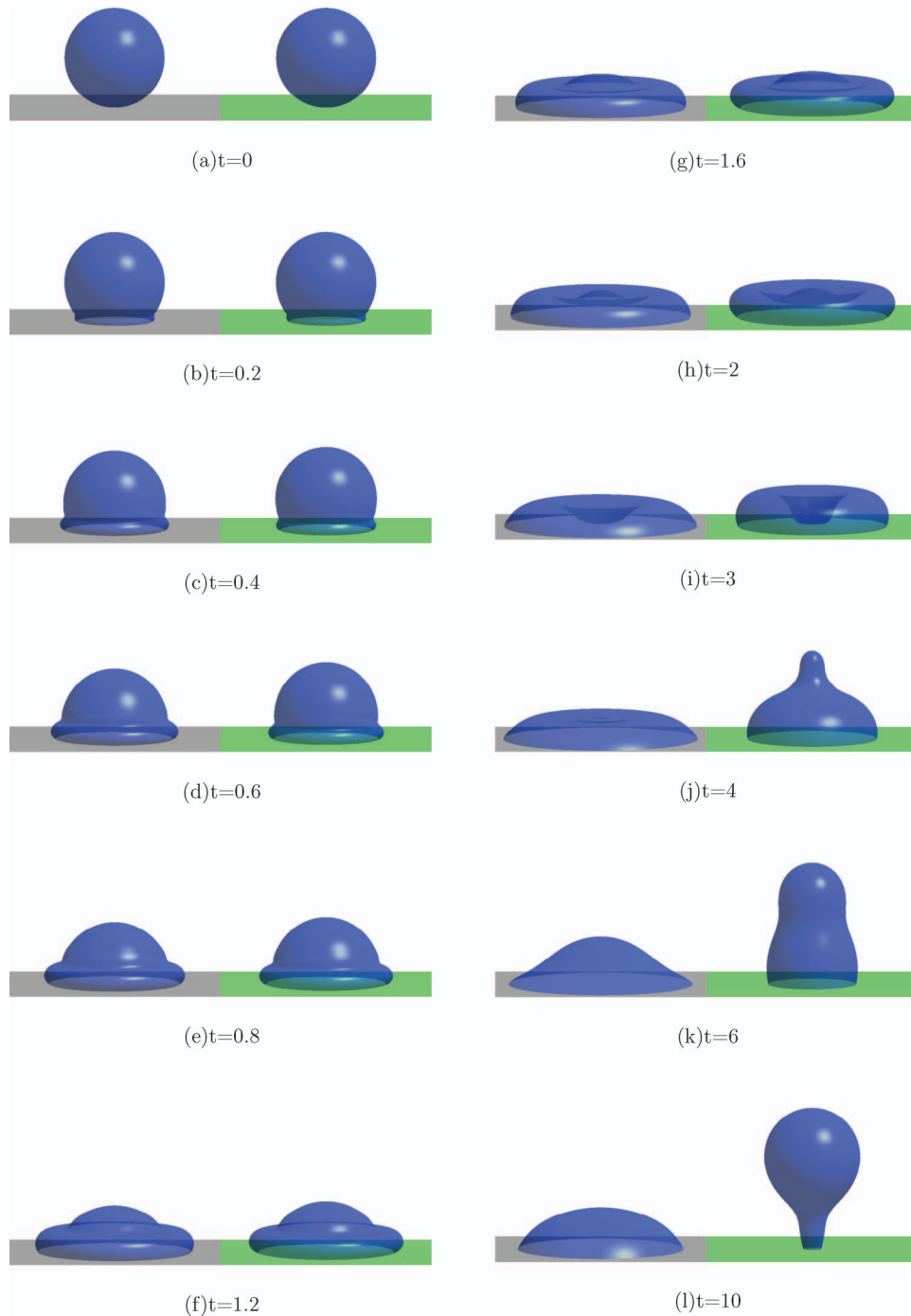
FIG. 3. Microdrop impact and spreading simulations at $Re = 130$, $Ca = 0.07$, and $St = 0.001$. The substrate on the left is hydrophilic ($\theta_e = 60°$) while the right is hydrophobic ($\theta_e = 130°$) (enhanced online)   [URL: http://dx.doi.org/10.1063/1.4739933.1].

As an illustration of the first of these advantages, as shown in Figures 5 and 7, in our simulations we are able to see the entire shape of the microdrop for the whole simulation, whereas experimental images on microdrops are unable to show the dynamics of the apex as it disappears below the rim of fluid which surrounds it, as well as features experimentally unobtainable at these scales such as the flow field and pressure distribution inside the drop. It can be seen that the apex gets extremely
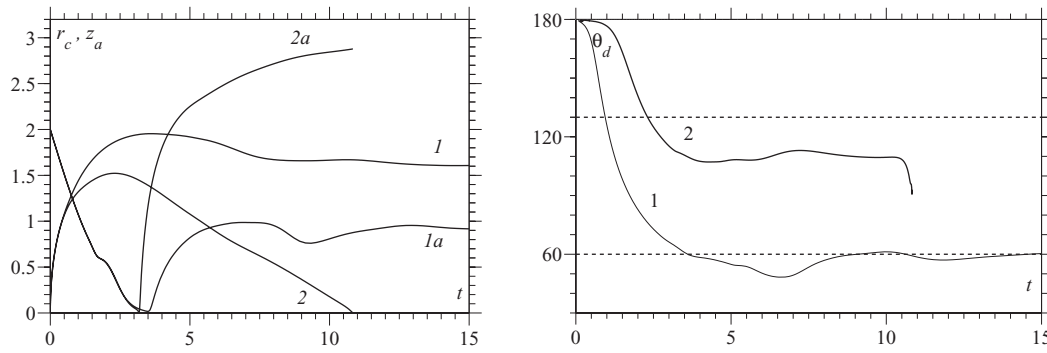
FIG. 4. Left: evolution of the drop's contact line position r_c (1, 2) and apex height z_a (1a, 2a) as a function of time for simulations at $Re = 130$, $Ca = 0.07$, and $St = 0.001$. Right: the corresponding values of the dynamic contact angle θ_d with the dashed lines corresponding to the equilibrium contact angles. Curves 1 and 1a: $\theta_e = 60°$ and curves 2 and 2a: $\theta_e = 130°$.
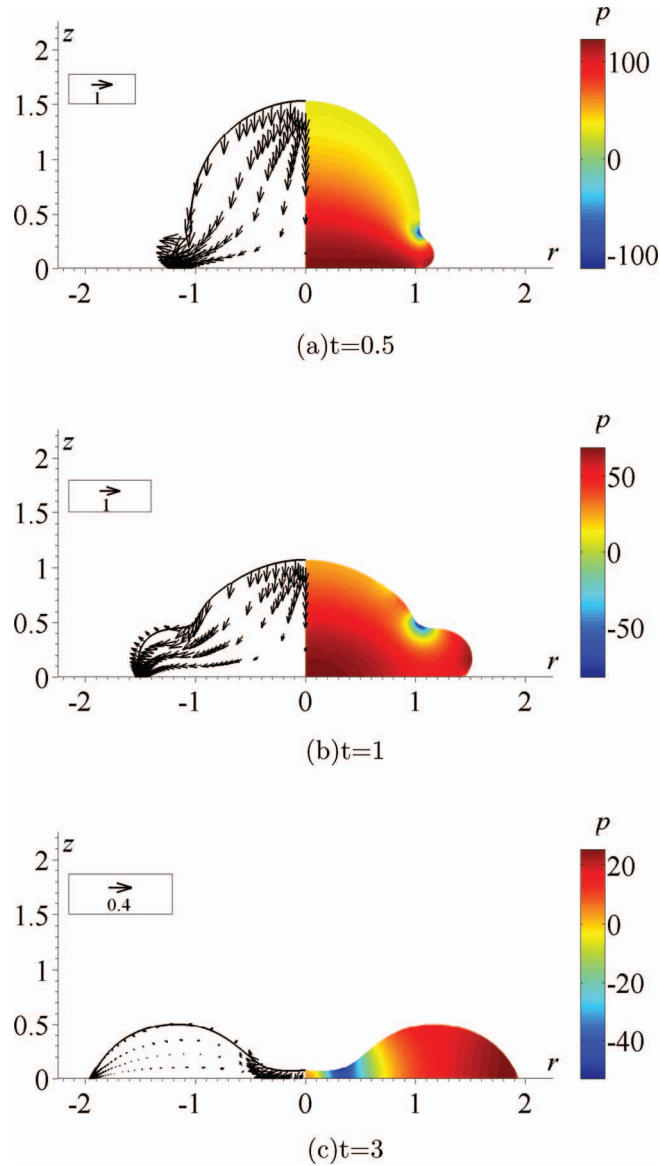

FIG. 5. Microdrop impact and spreading simulation at $Re = 130$, $Ca = 0.07$, and $St = 0.001$ on a hydrophilic substrate ($\theta_e = 60°$). Left: velocity vectors, and right: pressure field.
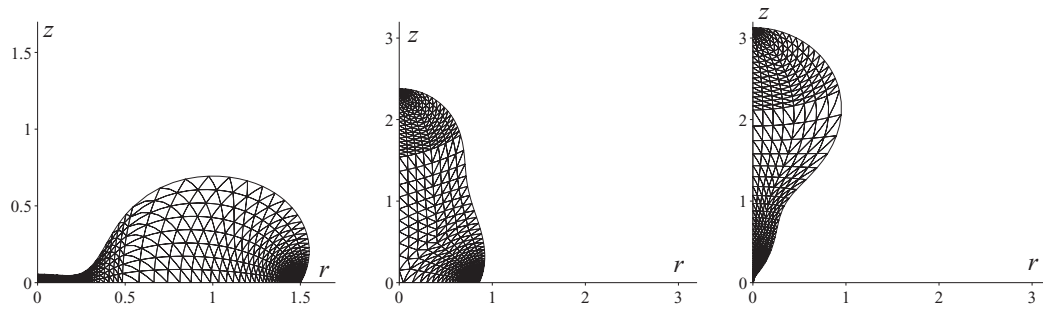
FIG. 6. Snapshots of a relatively coarse computational mesh during the impact, spreading, and rebound of the drop in Figure 3 off a hydrophobic substrate at times $t = 3, 6,$ and 10.5.

close to touching the solid substrate, i.e., to dewetting the centre of the drop. This can also be seen from curve $2a$ in Figure 4. The apex manages to recover just in time: as the contact line is receding, the apex re-emerges out of the centre of the drop in a jet-like protrusion (see Figure 3(j)). One could envisage that if the drop's apex does dewet the centre of the drop, then this additional dissipation of energy may inhibit the rebound of the drop off the hydrophobic surface, although, initial indications in the relatively narrow parameter space investigated thus far show that microdrops are remarkably resilient to this dewetting feature. Understanding, and hence being able to control, this feature would be of significant benefit to processes which are constrained to using hydrophobic surfaces but would like to inhibit rebound. This aspect of the drop impact phenomenon will be the subject of future investigation.

With regard to the second advantage of reliable numerical simulations of microdrops over experiment, determining for what parameter values a drop will rebound is an important piece of information, particularly when the substrate to be used in a given process has to be hydrophobic, and it is difficult to find this out from experiments where one cannot vary material parameters of the system independently. With our numerical tool, parameter space can be mapped quickly and efficiently, so that one can ensure the drop deposits on a given substrate by, say, artificially changing the viscosity of the liquid or reducing the impact speed of the drop. Changing the substrate for the same microdrop impact parameters, we see that, for example, at $\theta_e = 110°$, no rebound of the drop is observed.

Next, as an example of the code's cost-effectiveness with regard to the process, we consider the impact of drops on a chemically patterned surface which is custom built to enhance pre-determinable flow control on the drop's dynamics.

VI. MICRODROP IMPACT AND SPREADING ON CUSTOM BUILT CHEMICALLY PATTERNED SURFACES

Consider how topologically different patterns of wettability on a substrate can be used to gain a required level of flow control on a drop once it has been deposited. Here, one such pattern is considered with the aim of changing the final shape of a drop for the same liquid-solid combination by only slightly changing the impact speed, an outcome which is impossible on a homogeneous substrate. To do so, we pattern an otherwise wettable solid ($\theta_e = 60°$) with a circle of nonwettable substrate ($\theta_e = 110°$) of radius 1.52 times that of the drop's initial radius (Figure 8).

FIG. 7. Shape of the microdrops at $t = 3$ highlighting dynamics which are inaccessible to experiments.
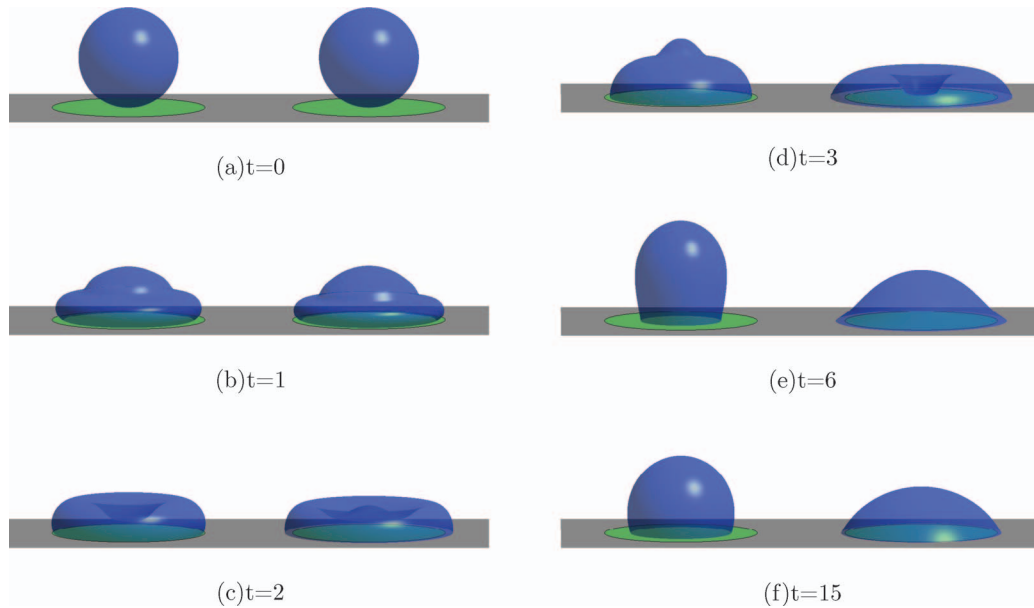
FIG. 8. Evolution of two drops impacting a patterned surface at (left) $U = 4$ m s^{-1} and (right) $U = 5$ m s^{-1}. The surface patterning is hydrophonic inside the circle (($r < 1.52$), $\theta_e = 110°$) and hydrophilic outside (($r > 1.52$), $\theta_e = 60°$) (enhanced online) [URL: http://dx.doi.org/10.1063/1.4739933.2].

From Figures 8 and 9, and the movie of the simulation shown in Video 2, we see how the desired flow control becomes realizable. On the patterned surface, the equilibrium radius of the area wetted by a drop impacting at 4 m s^{-1} is found to be $r_c = 1.03$, while for a 5 m s^{-1} impact, it is $r_c = 1.61$. This occurs because for the lower impacting speed the drop is unable to reach the edge of the hydrophobic area to access the more wettable region, and hence behaves as if it is on a homogeneous surface with wettability defined by $\theta_e = 110°$. For the higher speed of impact the drop is able to reach the edge of the hydrophobic disc, and encounter the more wettable substrate, as can be seen by looking at curve 2 in Figure 9 at $t = 2$. This results in an increase in the wetting speed and causes the contact line to advance further. There is no guarantee that the drop's contact line will remain on the more wettable surface as the contact line could return to the hydrophobic solid, which in turn would enhance the dewetting process. However, from curve 2 in Figure 9, we can see that the contact
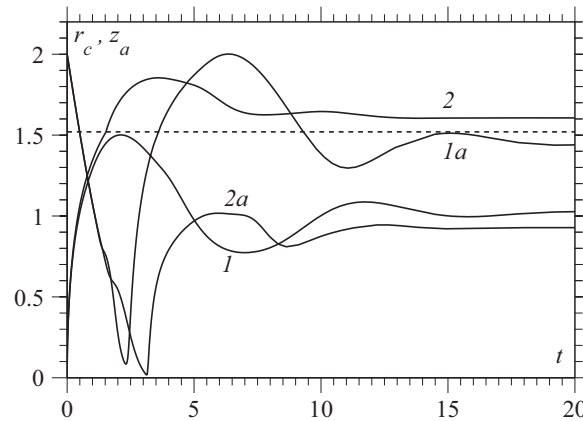

FIG. 9. Radius of the contact line (1, 2) and apex height (1a, 2a) as a function of time for two drops impacting a patterned surface at 1: $U = 4$ m s^{-1} and 2: $U = 5$ m s^{-1}, respectively. The boundary between the surface characterized by $\theta_e = 110°$ ($r < 1.52$) and that defined by $\theta_e = 60°$ ($r > 1.52$) is marked with a dashed line.

line's recoil is relatively shallow, and, in the case considered, it approaches an equilibrium position without ever encountering the hydrophobic disc again.

Thus, it has been shown that custom built substrates can be designed very quickly using our code to determine the specific details, such as the radius of the nonwettable inner circle. This is critical to the ability of a particular surface to carry out a given function, so that the experimental phase of optimizing such a product is significantly reduced. The pattern studied is just one of many that could be investigated, such as, for example, an annulus of wettability which could allow further control on the potential equilibrium shapes of the drop. However, the main new physical effect is the one considered here.

VII. CONCLUSION

The ability of the computational framework developed in Refs. 53 and 56, which, for the first time, implements in full the mathematical model of dynamic wetting as an interface formation process, to provide high-accuracy benchmark simulations for flows with large changes in free surface shape has been demonstrated. An initial study into the key physical effects of microdrop impact and spreading, applicable to the inkjet printing regime, has been performed, and the effect of the wettability of a substrate shown to be critical to the drop's dynamics, which can now be recovered in regimes hidden to experimental analysis. We have shown that the strong influence of the substrate's wettability on the drop's dynamics can be utilized to design chemically patterned surfaces allowing one to change considerably the final shape of the drop by only slightly altering the impact speed. This is an entirely new physical effect which deserves further investigation and fine tuning.

In this article, our focus has been on showing the capabilities of our computational platform and highlighting some of the key physical effects of microdrop impact and spreading. Future work will be concerned with comparing our results to both existing experimental data in the literature, with the initial simulations showing excellent agreement with those observed in Ref. 17, and, in parallel, using our code to design theory-driven experiments. The latter could identify parameter regimes in which bifurcations in the flow behaviour occur, such as rebound of the drop, dewetting of the centre, etc, and highlight where the differences between the predictions of models proposed in the literature for dynamic wetting will be most prominent.

The finite element framework developed has already been shown to possess reasonable flexibility: it was used to consider flow over patterned surfaces,[24,25] to simulate two-phase flow through a capillary[53,56] and here it was used to study the dynamics of free drops and their interaction with solid surfaces of varying types. This flexibility allows our research programme to branch out and simulate a whole array of different dynamic wetting flows, e.g., the coating of fibres,[71] where the high speeds of coating in confined areas suggest "hydrodynamic resist"[53] may be present, or it can be applied to entirely different flows where interface formation has also been shown to be critical, such as the coalescence of liquid bodies, breakup of liquid jets, disintegration of thin films, and other phenomena.[29]

Finally, it should be mentioned that the key to the interface formation model's capability of describing "hydrodynamic assist of dynamic wetting" as well as its opposite, "hydrodynamic resist," i.e., summarily, the dependence of the dynamic contact angle on the flow field, is that in this model the macroscopic description of the interface formation kinetics is intrinsically embedded into the fluid dynamics of the interfaces and the bulk. If the interface formation is treated separately from the fluid dynamics, as for example in the well-known molecular-kinetic theory,[72] which considers essentially the same physics of interface formation as an adsorption-desorption process in the framework of Eyring's reaction rate approach, then the result will be an equation relating the dynamic contact angle only with the contact-line speed. If this self-contained equation is subsequently incorporated into fluid mechanics, then one will still need to address the non-integrable shear-stress singularity at the contact line, and the end result will be a "slip" model. This model will have a more meaningful angle-versus-speed relationship than most slip models, with physically transparent material constants, but this does not change the matter in principle: the "hydrodynamic assist/resist of dynamic wetting" will not be there. This intrinsic shortcoming inherent in the "bottom-up" molecular-kinetic approach is well known and, although attempts have been made to rectify it in the context of dynamic wetting,[73]

the problem remains unresolved, as it essentially requires the kinetic theory of liquids (as opposed to rarefied gases) to be developed. However, the molecular-kinetic theory can be very useful in the situations where there is no hydrodynamic assist/resist, as it can help to elucidate the link between the material constants involved in the macroscopic description of the interface formation process and the underlying microscopic ones.[60] The discussions of how various modelling approach interact can be found, for example, in Refs. 27, 29, 30, 73, and 74.

ACKNOWLEDGMENTS

[1] W. M. Grissom and F. A. Wierum, "Liquid spray cooling of a heated surface," Int. J. Heat Mass Transfer **24**, 261–271 (1981).

[2] V. Bergeron and D. Quéré, "Water droplets make an impact," Phys. World, May, 27–31 (2001).

[3] D. Attinger, Z. Zhao, and D. Poulikakos, "An experimental study of molten microdroplet surface deposition and solidification: Transient behavior and wetting angle dynamics," J. Heat Transfer **122**, 544–546 (2000).

[4] M. B. Lesser and J. E. Field, "The impact of compressible liquids," Annu. Rev. Fluid Mech. **15**, 97–122 (1983).

[5] M. Rein, "Phenomena of liquid drop impact on solid and liquid surfaces," Fluid Dyn. Res. **12**, 61–93 (1993).

[6] A. L. Yarin, "Drop impact dynamics: Splashing, spreading, receding, bouncing," Annu. Rev. Fluid Mech. **38**, 159–192 (2006).

[7] R. Rioboo, M. Marengo, and C. Tropea, "Time evolution of liquid drop impacts onto solid, dry surfaces," Exp. Fluids **33**, 112–124 (2002).

[8] T. M. Squires and S. R. Quake, "Microfluidics: Fluid physics at the nanoliter scale," Rev. Mod. Phys. **77**, 977–1026 (2005).

[9] F. Gao and A. A. Sonin, "Precise deposition of molten microdrops: The physics of digital microfabrication," Proc. R. Ir. Acad. A, Math. Phys. Sci. **444**, 533–554 (1994).

[10] C. M. Hong and S. Wagner, "Inkjet printed copper source/drain metallization for amorphous silicon thin-film transistors," IEEE Electron Device Lett. **21**, 384–386 (1999).

[11] P. Calvert, "Inkjet printing for materials and devices," Chem. Mater. **13**, 3299–3305 (2001).

[12] S. E. Burns, P. Cain, J. Mills, J. Wang, and H. Sirringhaus, "Inkjet printing of polymer thin-film transistor circuits," MRS Bull. **28**, 829–834 (2003).

[13] M. Singh, H. Haverinen, P. Dhagat, and G. Jabbour, "Inkjet printing process and its applications," Adv. Mater. **22**, 673–685 (2010).

[14] B. Derby, "Inkjet printing of functional and structural materials: Fluid property requirements, feature stability and resolution," Annu. Rev. Mater. Res. **40**, 395–414 (2010).

[15] Y. Renardy, S. Popinet, L. Duchemin, M. Renardy, S. Zaleski, C. Josserand, M. A. Drumright-Clarke, D. Richard, C. Clanet, and D. Quéré, "Pyramidal and toroidal water drops after impact on a solid surface," J. Fluid Mech. **484**, 69–83 (2003).

[16] U. Mock, T. Michel, C. Tropea, I. V. Roisman, and J. Rühe, "Drop impact on chemically structured arrays," J. Phys.: Condens. Matter **17**, 595–605 (2005).

[17] H. Dong, W. W. Carr, D. G. Bucknall, and J. F. Morris, "Temporally-resolved inkjet impaction on surfaces," AIChE J. **53**, 2606–2617 (2007).

[18] D. B. van Dam and C. Le Clerc, "Experimental study of the impact of an inkjet printed droplet on a solid substrate," Phys. Fluids **16**, 3403–3414 (2004).

[19] R. Bhardwaj and D. Attinger, "Non-isothermal wetting during impact and millimeter-size water drop on a flat substrate: Numerical investigation and comparison with high-speed visualization experiments," Int. J. Heat Fluid Flow **29**, 1422–1435 (2008).

[20] J. Perelaer, P. J. Smith, E. van den Bosch, S. S. C. van Grootel, P. H. M. J. Ketelaars, and U. S. Schubert, "The spreading of inkjet-printed droplets with varying polymer molar mass on a dry solid substrate," Macromol. Chem. Phys. **210**, 495–502 (2009).

[21] A. Clarke, T. D. Blake, K. Carruthers, and A. Woodward, "Spreading and imbibition of liquid droplets on porous surfaces," Langmuir **18**, 2980–2984 (2002).

[22] R. K. Holman, M. J. Cima, S. A. Uhland, and E. Sachs, "Spreading and infiltration of ink-jet printed polymer solution droplets on a porous substrate," J. Colloid Sci. **249**, 432–440 (2002).

[23] T. Lim, S. Han, J. Chung, J. T. Chung, and S. Ko, "Experimental study on spreading and evaporation of inkjet printed pico-liter droplet on a heated substrate," Int. J. Heat Mass Transfer **52**, 431–441 (2009).

[24] J. E. Sprittles and Y. D. Shikhmurzaev, "Viscous flow over a chemically patterned surface," Phys. Rev. E **76**, 021602 (2007).

[25] J. E. Sprittles and Y. D. Shikhmurzaev, "A continuum model for the flow of thin liquid films over intermittently chemically patterned surfaces," Eur. Phys. J. Spec. Top. **166**, 159–163 (2009).

[26] E. B. Dussan, "On the spreading of liquids on solid surfaces: Static and dynamic contact lines," Annu. Rev. Fluid Mech. **11**, 371–400 (1979).

[27] T. D. Blake, "The physics of moving wetting lines," J. Colloid Interface Sci. **299**, 1–13 (2006).

[28] P. G. de Gennes, "Wetting: Statics and dynamics," Rev. Mod. Phys. **57**, 827–863 (1985).

[29] Y. D. Shikhmurzaev, *Capillary Flows with Forming Interfaces* (Chapman and Hall/CRC, Boca Raton, 2007).

[30] Y. D. Shikhmurzaev, "Some dry facts about dynamic wetting," Eur. Phys. J. Spec. Top. **197**, 47–60 (2011).

[31] C. Huh and L. E. Scriven, "Hydrodynamic model of steady movement of a solid/liquid/fluid contact line," J. Colloid Interface Sci. **35**, 85–101 (1971).

[32] Y. D. Shikhmurzaev, "Singularities at the moving contact line: Mathematical, physical and computational aspects," Physica D **217**, 121–133 (2006).

[33] C. L. M. H. Navier, "Mémoire sur les lois mouvement des fluides," Mém. de l'Acad. de Sciences l'Inst. de France **6**, 389–440 (1823).

[34] H. P. Greenspan, "On the motion of a small viscous droplet that wets a surface," J. Fluid Mech. **84**, 125–143 (1978).

[35] M. Pasandideh-Fard, Y. M. Qiao, S. Chandra, and J. Mostaghimi, "Capillary effects during droplet impact on a solid surface," Phys. Fluids **8**, 650–659 (1996).

[36] K. Yokoi, D. Vadillo, J. Hinch, and I. Hutchings, "Numerical studies of the influence of the dynamic contact angle on a droplet impacting on a dry surface," Phys. Fluids **21**, 072102 (2009).

[37] I. S. Bayer and C. M. Megaridis, "Contact angle dynamics in droplets impacting on flat surfaces with different wetting characteristics," J. Fluid Mech. **558**, 415–449 (2006).

[38] Š. Šikalo, H. D. Wilhelm, I. V. Roisman, S. Jakirlić, and C. Tropea, "Dynamic contact angle of spreading droplets: Experiments and simulations," Phys. Fluids **17**, 062103 (2005).

[39] T. D. Blake, A. Clarke, and K. J. Ruschak, "Hydrodynamic assist of wetting," AIChE J. **40**, 229–242 (1994).

[40] T. D. Blake, M. Bracke, and Y. D. Shikhmurzaev, "Experimental evidence of nonlocal hydrodynamic influence on the dynamic contact angle," Phys. Fluids **11**, 1995–2007 (1999).

[41] A. Clarke and E. Stattersfield, "Direct evidence supporting nonlocal hydrodynamic influence on the dynamic contact angle," Phys. Fluids **18**, 048106 (2006).

[42] C. G. Ngan and E. B. Dussan V, "On the nature of the dynamic contact angle: An experimental study," J. Fluid Mech. **118**, 27–40 (1982).

[43] V. D. Sobolev, N. V. Churaev, M. G. Velarde, and Z. M. Zorin, "Surface tension and dynamic contact angle of water in thin quartz capillaries," J. Colloid Interface Sci. **222**, 51–54 (2000).

[44] V. D. Sobolev, N. V. Churaev, M. G. Velarde, and Z. M. Zorin, "Dynamic contact angles of water in ultrathin capillaries," Colloid J. **63**, 119–123 (2001).

[45] P. G. Simpkins and V. J. Kuck, "On air entrainment in coatings," J. Colloid Interface Sci. **263**, 562–571 (2003).

[46] M. C. T. Wilson, J. L. Summers, Y. D. Shikhmurzaev, A. Clarke, and T. D. Blake, "Nonlocal hydrodynamic influence on the dynamic contact angle: Slip models versus experiment," Phys. Rev. E **83**, 041606 (2006).

[47] Y. D. Shikhmurzaev, "The moving contact line on a smooth solid surface," Int. J. Multiphase Flow **19**, 589–610 (1993).

[48] Y. D. Shikhmurzaev, "Moving contact lines in liquid/liquid/solid systems," J. Fluid Mech. **334**, 211–249 (1997).

[49] Y. D. Shikhmurzaev, "Spreading of drops on solid surfaces in a quasi-static regime," Phys. Fluids **9**, 266–275 (1996).

[50] Y. D. Shikhmurzaev, "Capillary breakup of liquid threads: A singularity-free solution," IMA J. Appl. Math. **70**, 880–907 (2005).

[51] Y. D. Shikhmurzaev, "Macroscopic mechanism of rupture of free liquid films," C. R. Mec. **333**, 205–210 (2005).

[52] Y. D. Shikhmurzaev, "Singularity of free-surface curvature in convergent flow: Cusp or corner?," Phys. Lett. A **345–385**, 378 (2005).

[53] J. E. Sprittles and Y. D. Shikhmurzaev, "Finite element framework for simulating dynamic wetting flows as an interface formation process," J. Comput. Phys. (in press).

[54] N. V. Priezjev, A. A. Darhuber, and S. M. Troian, "Slip behaviour in liquid films on surfaces of patterned wettability: Comparison between continuum and molecular dynamics simulations," Phys. Rev. E **71**, 041608 (2005).

[55] T. Qian, X. Wang, and P. Sheng, "Hydrodynamic slip boundary condition at chemically patterned surfaces: A continuum deduction from molecular dynamics," Phys. Rev. E **72**, 022501 (2005).

[56] J. E. Sprittles and Y. D. Shikhmurzaev, "A finite element framework for describing dynamic wetting phenomena," Int. J. Numer. Methods Fluids **68**, 1257–1298 (2012).

[57] E. W. Washburn, "The dynamics of capillary flow," Phys. Rev. **17**, 273–283 (1921).

[58] S. Hysing, "Numerical simulation of immiscible fluids with FEM level set techniques," Ph.D. dissertation (Institute of Applied Mathematics, University of Dortmund, 2007).

[59] T. Young, "An essay on the cohesion of fluids," Philos. Trans. R. Soc. London **95**, 65–87 (1805).

[60] T. D. Blake and Y. D. Shikhmurzaev, "Dynamic wetting by liquids of different viscosity," J. Colloid Interface Sci. **253**, 196–202 (2002).

[61] S. F. Kistler, and L. E. Scriven, "Coating flows," in *Computational Analysis of Polymer Processing*, edited by J. R. A. Pearson and S. M. Richardson (Applied Science, London/New York, 1983), pp. 243–299.

[62] M. Heil "An efficient solver for the fully-coupled solution of large displacement fluid-structure interaction problems," Comput. Methods Appl. Mech. Eng. **193**, 1–23 (2004).

[63] P. Lötstedt and L. Petzold, "Numerical solution of nonlinear differential equations with an algebraic constraints 1: Convergence results for backward differentiation formulas," Math. Comput. **46**, 491–516 (1986).

[64] P. M. Gresho and R. L. Sani, *Incompressible Flow and the Finite Element Method. Volume 2. Isothermal Laminar Flow* (Wiley, New York, 1999).

[65] J. W. Rayleigh, "On the capillary phenomena of jets," Proc. R. Soc. London **20**, 71–97 (1879).

[66] O. A. Basaran, "Nonlinear oscillations of viscous liquid drops," J. Fluid Mech. **241**, 169–198 (1992).

[67] S. Meradji, T. P. Lyubimova, D. V. Lyubimov, and B. Roux, "Numerical simulation of a liquid drop freely oscillating," Cryst. Res. Technol. **36**, 729–744 (2001).

[68] T. G. Wang, A. V. Anilkumar, and C. P. Lee, "Oscillations of liquid drops: Results from USML-1 experiments in space," J. Fluid Mech. **308**, 1–14 (1996).

[69] W. R. Smith, "Modulation equations for strongly nonlinear oscillations of an incompressible viscous drop," J. Fluid Mech. **654**, 141–159 (2010).

[70] T. Mao, D. C. S. Kuhn, and H. Tran, "Spread and rebound of liquid droplets upon impact on flat surfaces," AIChE J. **43**, 2169–2179 (1997).

[71] S. Ravinutala and C. Polymeropoulos, "Entrance meniscus in a pressurized optical fiber coating applicator," Exp. Therm. Fluid Sci. **26**, 573–580 (2002).

[72] T. D. Blake and J. M. Haynes, "Kinetics of liquid/liquid displacement," J. Colloid Interface Sci. **30**, 421–423 (1969).

[73] T. D. Blake, "Dynamic contact angles and wetting kinetics," in *Wettability*, edited by J. C. Berg (Marcel Dekker, 1993), pp. 251–309.

[74] T. D. Blake and J. De Coninck, "The influence of solid-liquid interactions on dynamic wetting," Adv. Colloid Interface Sci. **66**, 21–36 (2002).